

**UCSF**

**UC San Francisco Previously Published Works**

**Title**

High-resolution Imaging in Male Germ Cell-Associated Kinase (MAK)-related Retinal Degeneration

**Permalink**

<https://escholarship.org/uc/item/3sw1n5db>

**Authors**

Lew, Young Ju  
Rinella, Nicholas  
Qin, Jia  
[et al.](#)

**Publication Date**

2018

**DOI**

10.1016/j.ajo.2017.10.023

Peer reviewed



Published in final edited form as:

*Am J Ophthalmol.* 2018 January ; 185: 32–42. doi:10.1016/j.ajo.2017.10.023.

## High Resolution Imaging in male germ cell associated kinase (MAK)-related Retinal Degeneration

Young Ju Lew<sup>1</sup>, Nicholas Rinella<sup>1</sup>, Jia Qin<sup>1</sup>, Joanna Chiang<sup>1</sup>, Anthony T. Moore<sup>1</sup>, Travis C. Porco<sup>1,2,3</sup>, Austin Roorda<sup>4</sup>, and Jacque L. Duncan<sup>1</sup>

<sup>1</sup>Department of Ophthalmology, University of California, San Francisco, San Francisco, CA, USA

<sup>2</sup>Proctor Foundation, University of California, San Francisco, San Francisco, CA, USA

<sup>3</sup>Department of Epidemiology and Biostatistics, University of California, San Francisco, San Francisco, CA, USA

<sup>4</sup>School of Optometry and Vision Science Graduate Group, University of California, Berkeley, Berkeley, CA, USA

### Abstract

**Purpose**—To describe the characteristics of *MAK*-related retinal degeneration using optical coherence tomography angiography (OCTA) and adaptive optics scanning laser ophthalmoscopy (AOSLO).

**Design**—Cross-sectional study.

**Methods**—Six patients with rod-cone degeneration and disease-causing mutations in *MAK* were evaluated with visual acuity, spectral domain OCT, confocal AOSLO and OCTA. Foveal avascular zone (FAZ) area, vessel densities and perfusion densities of the superficial capillary plexus (SCP) and deep capillary plexus (DCP) in the central macula in all 6 patients were compared with 5 normal subjects. Cone spacing was measured in 4 patients from AOSLO images and compared with 37 normal subjects.

---

Corresponding author: Jacque L. Duncan, Department of Ophthalmology, University of California, San Francisco, 10 Koret Way, K113, San Francisco, CA 94143-0730, Phone: 415-514-4241, Fax: 415-476-0709, jacque.duncan@ucsf.edu. Young Jew Lew is now at Department of Ophthalmology, Kim's Eye Hospital, Seoul, Korea. Jia Qin is now at Foshan University, Foshan, Guangdong, China.

b. Financial disclosures: Young Ju Lew, none; Nicholas Rinella, none; Jia Qin, none; Joanna Chiang, none; Travis C. Porco, none; Austin Roorda holds 2 patents on technology related to the Adaptive Optics Scanning Laser Ophthalmoscope (USPTO #7,118,216 #6,890,076). These patents are assigned to both the University of Rochester and the University of Houston. The patents are currently licensed to Canon, Inc., Japan. Both Roorda and the company may benefit financially from the publication of this research; Jacque L. Duncan serves on the data safety monitoring board for clinical trials sponsored by Spark Therapeutics, Inc. (Philadelphia, PA, USA), AGTC, Inc. (Alachua, FL, USA), and The California Institute for Regenerative Medicine (Oakland, CA, USA). She is on the Scientific Advisory Board of SparingVision (Paris, France). She serves as Chair of the Scientific Advisory Board for The Foundation Fighting Blindness (Columbia, MD, USA). She has served as a consultant to Novelion Therapeutics (Vancouver, BC, Canada), Ionis Pharmaceuticals, Inc. (Carlsbad, CA, USA), Ocugen, Inc. (Malvern, PA, USA), Shire (Lexington, MA, USA), and Editas Medicine, Inc (Cambridge, MA, USA). She receives material support for an unrelated clinical trial from Neurotech Pharmaceuticals, Inc. (Cumberland, RI, USA).

**Publisher's Disclaimer:** This is a PDF file of an unedited manuscript that has been accepted for publication. As a service to our customers we are providing this early version of the manuscript. The manuscript will undergo copyediting, typesetting, and review of the resulting proof before it is published in its final citable form. Please note that during the production process errors may be discovered which could affect the content, and all legal disclaimers that apply to the journal pertain.

**Results**—Patients ranged from 25 to 81 years (mean, 52). Visual acuity varied from 20/13 to 20/40<sup>+2</sup>, except in one patient with cystoid macular edema whose vision was 20/60<sup>-</sup> and 20/70<sup>+1</sup>. The SCP ( $P=0.012$ ) and DCP ( $P=0.013$ ) vessel density and perfusion density ( $P=0.015$  and 0.013, respectively) were significantly lower in patients compared to normal subjects in the parafoveal region 1.0–3.0 mm from the fovea, but were similar to normal subjects within 1.0 mm of the fovea. The FAZ area was not significantly different from normal (all  $P>0.24$ ). Cone spacing was normal at almost all locations in 2 patients with early disease and increased in 2 patients with advanced disease.

**Conclusions**—Although retinal vascular densities are reduced and cone spacing is increased in advanced disease, central foveal structure is maintained until late stages of disease, which may contribute to preservation of foveal vision in eyes with *MAK*-related retinal degeneration.

## Table of Contents Statement

Six patients with rod-cone degeneration and mutations in the *male germ cell associated kinase (MAK)* gene were imaged using optical coherence tomography angiography and adaptive optics scanning laser ophthalmoscopy. Superficial and deep capillary plexus densities were not significantly different from normal within 1.0 mm of the fovea. Central foveal structure is maintained until late stages of disease in eyes with *MAK*-related retinal degeneration, which may contribute to preservation of foveal vision.

## Keywords

retinal degeneration; inherited retinal degeneration; retinitis pigmentosa; *MAK* gene; vessel density; cone photoreceptor; optical coherence tomography angiography (OCTA); adaptive optics scanning laser ophthalmoscopy (AOSLO)

## Introduction

Inherited retinal degenerations cause relentless, progressive loss of vision through a variety of mechanisms, affecting photoreceptors, retinal pigment epithelial (RPE) cells and vascular perfusion of the retina or choroid. Retinitis pigmentosa (RP) is one of the most common inherited retinal degenerations; patients with RP typically present with nyctalopia followed by progressive constriction of visual field and eventual loss of central vision.<sup>1–3</sup> Inherited retinal degenerations display heterogeneity in phenotype and genotype.<sup>2</sup> Well over 300 genes have been implicated so far and mutations in more than 80 genes have been associated with RP (<https://sph.uth.edu/retnet/sum-dis.htm>, accessed July 29, 2017).<sup>2, 4</sup>

Histopathologic studies of eyes from subjects with RP, donated after death, show progressive loss of photoreceptors and RPE cells, as well as extensive vascular and neural remodeling in the retina and choroid.<sup>5–7</sup> Although it is possible to study vascular changes in RP patients with fluorescein and indocyanine green angiography, both have the disadvantages of exposure to intravenous dye, and limited resolution incapable of imaging the finest capillaries.<sup>8</sup> Optical coherence tomography angiography (OCTA) noninvasively provides high-resolution images of the capillary network and the foveal avascular zone.<sup>8, 9</sup> Quantification of microvascular structures such as vascular densities and avascular zone areas has been reported using OCTA in normal eyes and in various retinal diseases.<sup>10–12</sup> In

RP, vascular densities of the superficial and deep retinal capillary plexus are reported to be significantly decreased compared to normal subjects.<sup>13–17</sup>

Adaptive optics scanning laser ophthalmoscopy (AOSLO) uses adaptive optics (AO) to compensate for optical aberrations, permitting observation of cellular structures in living human eyes.<sup>18, 19</sup> Confocal AOSLO images reveal retinal microstructures that directly backscatter light, such as the nerve fiber layer, photoreceptors, RPE cells, and retinal vasculature.<sup>18, 20–22</sup> AOSLO has been used to characterize photoreceptor structure in healthy eyes and in eyes with inherited retinal degeneration.<sup>23–25</sup>

Autosomal recessive RP associated with mutations in the male germ cell associated kinase (*MAK*) gene is associated with preservation of the foveal vision even in advanced stages of retinal degeneration despite similar rates of peripheral visual field loss to other forms of autosomal recessive RP.<sup>7</sup> However, cystoid macular edema (CME) and intraretinal cystoid spaces (ICS) can occur which can reduce visual acuity.<sup>26</sup> In mice, *MAK* is involved in outer segment morphogenesis, regulation of connecting cilium length and photoreceptor survival.<sup>27</sup> *MAK* is expressed in the inner segments, cell bodies and axons of human photoreceptors, including foveal cones.<sup>28</sup> Although *MAK* has not been identified in vascular tissues, RPE and choriocapillaris atrophy has been reported in patients with *MAK*-related RP.<sup>7, 29</sup> In this study we used high-resolution OCTA and AOSLO to investigate the hypothesis that preserved retinal vasculature and cone spacing near the fovea may contribute to preservation of foveal vision in eyes with *MAK*-related RP.

## Methods

### Study Participants

The study and data collection were carried out with approval from the UCSF Institutional Review Board in a prospective manner. Informed consent was obtained and the study was in accordance with HIPAA regulations. This institutional, cross-sectional study included 5 patients from 5 families with rod-cone degeneration and 1 asymptomatic sibling (I-2, 40126; sibling of I-1, 40116). All subjects underwent genetic testing which revealed disease-causing mutations in the *MAK* gene. Patients were clinically evaluated with visual acuity measured according to the Early Treatment of Diabetic Retinopathy Study (ETDRS) protocol,<sup>30</sup> kinetic perimetry using a Goldmann perimeter, full-field electroretinography according to the International Society for Clinical Electrophysiology of Vision,<sup>31</sup> color fundus photos (TRC 50DX, Topcon Medical Systems, Inc., Oakland, NJ) in 4 of the 6 patients, spectral domain optical coherence tomography (SDOCT) and infrared photos in all 6 patients and fundus autofluorescence fundus images (Spectralis HRA+OCT; Heidelberg Engineering, Vista, CA) in 1 of the 6 patients, and high resolution retinal images using a swept-source OCTA system, and a custom-designed confocal AOSLO as described below in 4 of the 6 patients. Five normal subjects were imaged for the vessel density analysis, while previously reported cone spacing data from 37 normal eyes were used to compare with cone spacing measures from patients.<sup>32</sup>

## Optical Coherence Tomography Angiography (OCTA)

OCTA was performed using a swept-source system (PLEX Elite 9000, Carl Zeiss Meditec, Inc., Dublin, CA); the technical aspects of the system have been described elsewhere.<sup>33</sup> Briefly, the system provides transverse imaging resolution of 15  $\mu\text{m}$ , with a central wavelength of 1060 nm and a speed of 100,000 A-scans per second. Three dimensional OCTA slab images were formed by scanning a 3 mm  $\times$  3 mm area consisting of 300 A-scans per B-scan, and 300 B-scans were obtained in a horizontal raster pattern with each B-scan repeated 4 times consecutively with a scanning depth of 3 mm over 1536 pixels.

Quantitative analyses of the FAZ and vessel density at the level of the superficial capillary plexus (SCP) and deep capillary plexus (DCP) were performed using custom software in order to binarize and skeletonize the images.<sup>10, 12</sup> In order to quantify the vessel densities, all OCTA images were exported into the Advanced Retinal Imaging (ARI) collaboration network portal ([www.zeiss.com/arinetwork](http://www.zeiss.com/arinetwork)) (Tumlinson AR, et al., IOVS 2017;58:ARVO E-Abstract 1864). A thresholding algorithm was applied to the SCP and DCP *en face* images to create a binary slab that assigns to each pixel a 1 (perfused) or 0 (background). The skeletonized slab was created from this binary image. Using skeletonized images where each blood vessel was shown as a 1-pixel-wide line, vessel density was defined as the total length of perfused vasculature per unit area in a region of measurement. It was calculated by averaging regions of the skeletonized images in  $\text{mm}^{-1}$  [(pixels of vessels)  $\times$  (3 mm/300 pixels)/(area in a region of measurement in  $\text{mm}^2$ )].<sup>10, 34</sup> The average of the skeletonized slab is only a first-order estimate of the length of perfused vasculature. A more accurate calculation would require considering the relationship between neighboring pixels with value 1 in the skeletonized slab. Perfusion density was calculated as total area of perfused vessels observed per unit area, producing a value ranging from 0 (nonperfused) to 1 (fully perfused); typical perfusion density values remain below 0.5. There may be sources of error in the perfusion density measurement, including the large transverse resolution as compared to the size of the smallest capillaries, and the sensitivity of the thresholding step in the binarization process to noise in the image. In particular, perfusion density may not be sensitive to changes in vessel caliber. But, vessels that are non-perfused should cause a reduction in the observed perfusion density as well as the vessel density, so both measures are expected to be reduced in the presence of capillary loss. To investigate foveal perfusion, we analyzed the central 1.0 mm surrounding the center of the FAZ separately from the parafoveal ring extending from 1.0–3.0 mm from the center of the FAZ for both the SCP and the DCP, and also analyzed the FAZ area, in patients and normal controls. The FAZ area was manually outlined in SCP and DCP images, calculated as pixels and converted to  $\text{mm}^2$  [(pixels of FAZ)  $\times$  (3 mm/300 pixels)<sup>2</sup>].<sup>10</sup>

## Adaptive Optics Scanning Laser Ophthalmoscopy (AOSLO)

High-resolution images of central macular cones were obtained using confocal AOSLO. The AOSLO uses a low coherence, 840 nm light source, a Shack-Hartmann wavefront sensor, and a 140-actuator microelectromechanical (MEMS) deformable mirror (Boston Micromachines Corporation, Watertown, MA, USA). Digital videos were recorded throughout the central macular area of 5.7° in diameter, centered on the fovea, and each video subtended an area of 1.2° square, as described previously.<sup>25, 35</sup> Images were processed

to create montages of the macular area. Cone spacing was measured as previously described.<sup>24, 36, 37</sup> Briefly, each region in which unambiguous cone mosaics were clearly visualized were selected as region of interest (ROI) for cone spacing measurements, and ROI location was measured as eccentricity in degrees relative to the preferred retinal locus.

### Genetic Analysis

Whole blood samples were collected from 6 patients, DNA was extracted and genetic testing was performed using next-generation sequencing panels (Jewish retinal dystrophy panel or genetic eye disease panel) with confirmatory Sanger sequencing on a fee-for-service basis (John and Marcia Carver Nonprofit Genetic Testing Laboratory, University of Iowa, Ames, IA, USA; Genetic Diagnostic Laboratory, Ocular Genomics Institute, Harvard Medical School, Boston, MA, USA; and Blueprint Genetics, Helsinki, Finland).<sup>7, 38</sup>

### Statistical analysis

All quantitative variables from OCTA were summarized as mean and standard deviation. Linear mixed effects regression was performed using R to compare normal subjects with patients for the vessel densities and perfusion densities within 1 mm of the fovea and in the ring between 1–3 mm from the fovea of the SCP and DCP, while Hotelling's  $T^2$  test was used to compare FAZ area measured in the SCP and DCP between normal subjects and patients. Cone spacing was compared to mean and 95% confidence intervals (CI) from 37 age-similar normal subjects that have been described previously.<sup>32</sup>

### Results

Six patients ranged in age from 25 to 81 years old (mean age, 52 years  $\pm$  21 years) and were similar in age to 5 normal control subjects ranging from 25–79 (mean age, 46 years  $\pm$  23) years (2 tailed  $t$ -test  $P=0.55$ ). Genetic tests revealed homozygous mutation of *MAK* in all patients (Table 1).

The clinical characteristics of patients are summarized in Table 1. The visual acuity varied from 20/13 to 20/70; patient P III had severe cystoid macular edema with vision reduced to 20/60 and 20/70. Kinetic perimetry showed temporal scotomas in 2 siblings (P 1-1, 40116 and P 1-2, 40126) with early disease, relatively preserved nasal fields in patient P III, a preserved temporal crescent in patient P II (40063), and central islands in patients P IV (40123) and P V (Figure 1).

We compared the vessel densities, perfusion densities and foveal avascular zone (FAZ) area of the SCP and DCP in the central macula from OCTA images in all 6 patients (12 eyes) with data from 5 age-similar normal subjects (10 eyes) (Table 2, Figure 2). Quantitative analysis of vessel density and perfusion density in the SCP and DCP was performed at the foveal (0 mm–1.0 mm) and parafoveal (1.0 mm–3.0 mm) regions (Figure 3). The FAZ area was not significantly different from normal ( $P=0.80$ ) and the SCP and DCP vessel density ( $P=0.53$  and  $0.98$ , respectively) and perfusion density ( $P=0.77$  and  $0.24$ , respectively) in regions from 0 mm – 1.0 mm from the fovea were not significantly lower in patients compared to normal subjects (Table 2). However, the SCP and DCP vessel density ( $P=0.012$  and  $0.014$ , respectively) and perfusion density ( $P=0.015$  and  $0.013$ , respectively) were

significantly lower in the parafoveal region extending from 1.0–3.0 mm from the fovea in patients compared to normal subjects. Excluding the patient with cystoid macular edema (P III) did not change the values significantly; SCP and DCP vessel densities ( $P=0.024$  and  $0.025$ , respectively) and perfusion densities ( $P=0.025$  and  $0.020$ , respectively) in the parafoveal region from 1.0–3.0 mm from the fovea were still significantly lower in patients with *MAK*-related retinal degeneration than normal subjects. The parafoveal vessel density and perfusion densities of both the SCP and DCP were more reduced in *MAK* patients, while FAZ area, vessel densities and perfusion densities within 1.0 degrees of the fovea were similar to normal subjects.

Cone spacing was measured in 8 eyes of 4 patients (P I-1, P I-2, P II and P IV) from AOSLO images and compared with normal cone spacing measures.<sup>32</sup> Cone spacing measures were within the 95% confidence intervals of normal mean values in 2 siblings with early stages of disease severity (P I-1, 40116 and P I-2, 40126). Cone spacing measures were greater than the upper 95% confidence limits of normal in 2 patients with advanced stages of disease severity (P II, 40063 and P IV, 40123) (Figures 4 and 5).

## Discussion

*MAK* has recently been identified as a common cause of autosomal recessive RP.<sup>7, 28, 29</sup> The phenotype in *MAK*-related RP is mild with preservation of visual acuity into late adult life; a similar mild phenotype is seen in autosomal dominant RP caused by mutations in the *RP-1* gene.<sup>3, 7</sup> Normal visual acuities have been reported in patients in the eighth decade of life and visual fields have shown preservation of the nasal field in early stages of disease, but only central islands remain in advanced stages of disease.<sup>3, 7</sup> In the present study, visual acuities were near normal even with advanced disease, except in a patient (P III) with bilateral cystoid macular edema (Figure 3). The prevalence of cystoid macular edema has been reported to range from 28–49% of RP,<sup>39–41</sup> and intraretinal cystoid spaces have been reported in *MAK*-related RP.<sup>26</sup> One of the 6 patients in the current study showed bilateral cystoid macular edema, suggesting that regular examination of retinal structure using OCT is necessary in *MAK* patients, especially when visual acuity is reduced.

High-resolution imaging including OCTA and AOSLO demonstrated differences of retinal vascular and cellular structure in *MAK*-related RP compared to normal subjects. Vascular changes during disease progression in RP, such as attenuation of retinal vessels, perivascular pigment deposits and retinal atrophy are common, nonspecific findings in many forms of RP.<sup>2</sup> Alteration in ocular blood flow and vessel diameter has been reported using laser Doppler flowmetry,<sup>42</sup> magnetic resonance imaging,<sup>43, 44</sup> and ocular pulse amplitude.<sup>45</sup> In RP patients, higher oxygen saturation than normal has been found using retinal oximetry, and decreased vessel diameter or decreased oxygen diffusion secondary to thickening of capillary basement membranes are considered possible causes.<sup>46, 47</sup> The cause of the structural and functional changes in retinal vessels is unclear, but may be a consequence of tissue atrophy and reduced oxygen consumption.<sup>14, 48</sup> However, measurement of blood flow and vessel diameter required methods which are impractical for widespread use in clinical settings.<sup>17</sup> OCTA provides images of different retinal capillary plexuses *in vivo* through vascular layer segmentation<sup>33</sup> and can be used to monitor vascular abnormalities during

disease progression. The large field of view of OCTA enables visualization of microvascular networks at varying stages of RP with high resolution.<sup>17</sup>

Recently, 2 studies reported quantitative analysis of vessel densities using OCTA in RP patients without reported genetic mutations.<sup>14, 15</sup> Both studies showed reduced parafoveal SCP and DCP densities compared to normal subjects, but choriocapillaris density values were abnormal only in 1 of the 2 studies,<sup>15</sup> perhaps due to different disease stages and genotypes between the studies. Analysis of choriocapillaris vessel densities is complicated by projection artifacts which appear in deeper retinal structures.<sup>49</sup> For this reason, we did not analyze vessel density at the level of the choriocapillaris. In the current study, FAZ area showed no significant difference compared to normal subjects, while a previous study which investigated FAZ area showed enlargement of the FAZ at the level of DCP in patients with RP of unknown genotype.<sup>14</sup> It is possible that the power to detect a difference between patients and normal subjects in vascular density in this region is limited by the fact that the central 1.0 mm includes the FAZ in which very few vessels are present within the 1 mm circle. However, preservation of the perifoveal capillaries, manifest as normal FAZ area, may contribute to or result from preservation of foveal vision and structure even in late stages of *MAK*-related RP.

Direct visualization of the cone mosaic in patients with retinal degeneration can provide insight into the effects on macular cones of retinal degenerations due to different genetic mutations.<sup>32, 36, 37, 50</sup> In healthy eyes, cones appear as bright spots arranged in a close-packed pattern with regular spacing, while in eyes with retinal degeneration cones can show abnormal morphology, including increased cone spacing, irregular packing and sparse cone mosaics in regions with extensive cone loss.<sup>36, 51–58</sup> Changes in cone spacing (average distance to the nearest neighboring cone) and cone density have been reported in various retinal diseases, and have been used to monitor cone structure during disease progression in longitudinal studies.<sup>37</sup> Cone spacing and density have been reported in cross-sectional studies of patients with inherited retinal degeneration to provide more sensitive measures of disease severity than visible changes on OCT or decline in visual acuity.<sup>32, 37, 57</sup> Cone spacing in 4 patients with *MAK*-related RP was within the limits of normal at almost all studied locations in 2 patients with early disease, indicating that significant cone loss had not occurred at this stage. In contrast increased spacing beyond the upper limits of normal was found in 2 patients with advanced disease. The 2 patients with early disease had a different mutation in the *MAK* gene than has been commonly reported, which may also contribute to the normal-appearing macular cone mosaics in these patients. However, the 2 patients with a *MAK* mutation that has been commonly reported in patients of Ashkenazi Jewish descent<sup>7</sup> showed cone spacing that was increased by greater than the 95% confidence intervals above the normal mean at advanced stages of disease, in the context of well-preserved visual acuity that was no worse than 20/32. Since cone spacing or cone density may change earlier than other outcome measures during disease progression, cone structural measures acquired from AOSLO images may provide a sensitive indicator of disease severity.

Our study has several limitations. First, the number of patients was small, but included patients with a range of age and disease severity. The results from this cross-sectional approach suggest that perifoveal vascular density and cone structure change during disease



progression despite the lack of prospective data. Second, image artifacts related to poor fixation or opaque media might influence image qualities of both OCTA and AOSLO. In this study, AOSLO images were not quantifiable in one patient with severe cystoid macular edema and another patient with pseudophakia, capsular phimosis and advanced disease, and our study is biased in not including cone spacing from patients with cystoid macular edema or media opacity. The density measures may be affected by noise and artifacts in the OCTA, and by limitations in resolution of the OCTA. The vessel density and perfusion density measures in this study were consistent, suggesting these potential sources of error did not significantly affect the observation of reduced vessel perfusion in patients with *MAK*-related RP. Finally, the correlation between structural and functional changes was not evaluated because of our limited sample size. Correlations between SCP and DCP density with both multifocal electroretinogram and ganglion cell complex thickness were reported in a previous cross-sectional study of RP patients.<sup>15</sup> Future longitudinal studies could determine which parameters are most useful to predict disease progression and provide additional insight into the relationship between structural abnormalities and visual function in *MAK*-related RP.

In summary, we have characterized the retinal microvasculature and cone structure in *MAK*-related RP using high-resolution images acquired with OCTA and AOSLO. High-resolution images using OCTA and AOSLO showed reduced SCP and DCP vessel density beginning at 1 degree eccentricity around the fovea, and increased cone spacing despite well-preserved visual acuity in eyes with advanced stages of disease. Foveal avascular zone area and vascular densities at fovea showed no significant difference compared to normal subjects, and this may contribute to preservation of foveal vision and structure even in late stages of disease in patients with *MAK*-related retinal degeneration. The findings are significant in that they demonstrate preserved foveal photoreceptor and vascular structure in advanced stages of disease, suggesting that patients may benefit from therapies to prolong photoreceptor survival even in advanced disease.

## Supplementary Material

Refer to Web version on PubMed Central for supplementary material.

## Acknowledgments

a. Funding/Support: This work was supported the National Institutes of Health [NIH Grants NIH EY002162, EY 024239]; the US Food and Drug Administration Office of Orphan Product Development [FDA R01-41001]; The Foundation Fighting Blindness, Columbia, MD; Research to Prevent Blindness, New York, NY [Nelson Trust Award for Retinitis Pigmentosa and unrestricted grant to UCSF]; The Bernard A. Newcomb Macular Degeneration Fund, San Francisco, CA; That Man May See, Inc., San Francisco, CA; Hope for Vision, Miami, FL; The Claire Giannini Fund, San Francisco, CA; The Larry L. Hillblom Foundation, Petaluma, CA [Research Network Grant 2014-A-003-NET], The Hedco Foundation, Danville, CA.

c. Other acknowledgements: We collaborated with Nathan Shemonski and Mary K. Durbin, Carl Zeiss Meditec, Inc. (Dublin, CA, USA), for OCTA analysis and manuscript revision.

## References

1. Berson EL. Retinitis pigmentosa. The Friedenwald Lecture. Invest Ophthalmol Vis Sci. 1993; 34(5): 1659–1676. [PubMed: 8473105]

2. Hartong DT, Berson EL, Dryja TP. Retinitis pigmentosa. *Lancet*. 2006; 368(9549):1795–1809. [PubMed: 17113430]
3. van Huet RA, Siemiakowska AM, Ozgul RK, et al. Retinitis pigmentosa caused by mutations in the ciliary MAK gene is relatively mild and is not associated with apparent extra-ocular features. *Acta Ophthalmol*. 2015; 93(1):83–94. [PubMed: 25385675]
4. Wright AF, Chakarova CF, Abd El-Aziz MM, Bhattacharya SS. Photoreceptor degeneration: genetic and mechanistic dissection of a complex trait. *Nat Rev Genet*. 2010; 11(4):273–284. [PubMed: 20212494]
5. Marc RE, Jones BW, Watt CB, Strettoi E. Neural remodeling in retinal degeneration. *Prog Retin Eye Res*. 2003; 22(5):607–655. [PubMed: 12892644]
6. Milam AH, Li ZY, Fariss RN. Histopathology of the human retina in retinitis pigmentosa. *Prog Retin Eye Res*. 1998; 17(2):175–205. [PubMed: 9695792]
7. Stone EM, Luo X, Heon E, et al. Autosomal recessive retinitis pigmentosa caused by mutations in the MAK gene. *Invest Ophthalmol Vis Sci*. 2011; 52(13):9665–9673. [PubMed: 22110072]
8. Schwartz DM, Fingler J, Kim DY, et al. Phase-variance optical coherence tomography: a technique for noninvasive angiography. *Ophthalmology*. 2014; 121(1):180–187. [PubMed: 24156929]
9. Jia Y, Tan O, Tokayer J, et al. Split-spectrum amplitude-decorrelation angiography with optical coherence tomography. *Opt Express*. 2012; 20(4):4710–4725. [PubMed: 22418228]
10. Iafe NA, Phasukkijwatana N, Chen X, Sarraf D. Retinal capillary density and foveal avascular zone area are age-dependent: quantitative analysis using optical coherence tomography angiography. *Invest Ophthalmol Vis Sci*. 2016; 57(13):5780–5787. [PubMed: 27792812]
11. Kang JW, Yoo R, Jo YH, Kim HC. Correlation of microvascular structures on optical coherence tomography angiography with visual acuity in retinal vein occlusion. *Retina*. 2017; 37(9):1700–1709. [PubMed: 27828907]
12. Li M, Yang Y, Jiang H, et al. Retinal microvascular network and microcirculation assessments in high myopia. *Am J Ophthalmol*. 2017; 174:56–67. [PubMed: 27818204]
13. Murakami Y, Ikeda Y, Akiyama M, et al. Correlation between macular blood flow and central visual sensitivity in retinitis pigmentosa. *Acta Ophthalmol*. 2015; 93(8):e644–648. [PubMed: 25688697]
14. Battaglia Parodi M, Cicinelli MV, Rabiolo A, et al. Vessel density analysis in patients with retinitis pigmentosa by means of optical coherence tomography angiography. *Br J Ophthalmol*. 2017; 101(4):428–432. [PubMed: 27343210]
15. Toto L, Borrelli E, Mastropasqua R, et al. Macular features in retinitis pigmentosa: correlations among ganglion cell complex thickness, capillary density, and macular function. *Invest Ophthalmol Vis Sci*. 2016; 57(14):6360–6366. [PubMed: 27898981]
16. Sugahara M, Miyata M, Ishihara K, et al. Optical coherence tomography angiography to estimate retinal blood flow in eyes with retinitis pigmentosa. *Sci Rep*. 2017; 7:46396. [PubMed: 28406171]
17. Rezaei KA, Zhang Q, Chen CL, Chao J, Wang RK. Retinal and choroidal vascular features in patients with retinitis pigmentosa imaged by OCT based microangiography. *Graefes Arch Clin Exp Ophthalmol*. 2017; 255(7):1287–1295. [PubMed: 28314954]
18. Roorda A, Duncan JL. Adaptive optics ophthalmoscopy. *Annu Rev Vis Sci*. 2015; 1:19–50. [PubMed: 26973867]
19. Roorda A, Romero-Borja F, Donnelly W III, Queener H, Hebert T, Campbell M. Adaptive optics scanning laser ophthalmoscopy. *Opt Express*. 2002; 10(9):405–412. [PubMed: 19436374]
20. Kurokawa K, Liu Z, Miller DT. Adaptive optics optical coherence tomography angiography for morphometric analysis of choriocapillaris [Invited]. *Biomed Opt Express*. 2017; 8(3):1803–1822. [PubMed: 28663867]
21. Mo S, Krawitz B, Efsthadiadis E, et al. Imaging foveal microvasculature: optical coherence tomography angiography versus adaptive optics scanning light ophthalmoscope fluorescein angiography. *Invest Ophthalmol Vis Sci*. 2016; 57(9):OCT130–140. [PubMed: 27409463]
22. Salas M, Augustin M, Ginner L, et al. Visualization of micro-capillaries using optical coherence tomography angiography with and without adaptive optics. *Biomed Opt Express*. 2017; 8(1):207–222. [PubMed: 28101412]

23. Duncan JL, Talcott KE, Ratnam K, et al. Cone structure in retinal degeneration associated with mutations in the peripherin/RDS gene. *Invest Ophthalmol Vis Sci.* 2011; 52(3):1557–1566. [PubMed: 21071739]
24. Yoon MK, Roorda A, Zhang Y, et al. Adaptive optics scanning laser ophthalmoscopy images in a family with the mitochondrial DNA T8993C mutation. *Invest Ophthalmol Vis Sci.* 2009; 50(4): 1838–1847. [PubMed: 18997096]
25. Zayit-Soudry S, Sippl-Swezey N, Porco TC, et al. Repeatability of Cone Spacing Measures in Eyes With Inherited Retinal Degenerations. *Invest Ophthalmol Vis Sci.* 2015; 56(10):6179–6189. [PubMed: 26416092]
26. Lai YH, Capasso JE, Kaiser R, Levin AV. Intraretinal cystoid spaces in a patient with retinitis pigmentosa due to mutation in the MAK gene. *Ophthalmic Genet.* 2016; 37(4):424–426. [PubMed: 26894652]
27. Omori Y, Chaya T, Katoh K, et al. Negative regulation of ciliary length by ciliary male germ cell-associated kinase (Mak) is required for retinal photoreceptor survival. *Proc Natl Acad Sci U S A.* 2010; 107(52):22671–22676. [PubMed: 21148103]
28. Tucker BA, Scheetz TE, Mullins RF, et al. Exome sequencing and analysis of induced pluripotent stem cells identify the cilia-related gene male germ cell-associated kinase (MAK) as a cause of retinitis pigmentosa. *Proc Natl Acad Sci U S A.* 2011; 108(34):E569–576. [PubMed: 21825139]
29. Ozgul RK, Siemiatkowska AM, Yucel D, et al. Exome sequencing and cis-regulatory mapping identify mutations in MAK, a gene encoding a regulator of ciliary length, as a cause of retinitis pigmentosa. *Am J Hum Genet.* 2011; 89(2):253–264. [PubMed: 21835304]
30. Ferris FL 3rd, Kassoff A, Bresnick GH, Bailey I. New visual acuity charts for clinical research. *Am J Ophthalmol.* 1982; 94(1):91–96. [PubMed: 7091289]
31. Marmor MF, Fulton AB, Holder GE, Miyake Y, Brigell M, Bach M. ISCEV Standard for full-field clinical electroretinography (2008 update). *Doc Ophthalmol.* 2009; 118(1):69–77. [PubMed: 19030905]
32. Ratnam K, Carroll J, Porco TC, Duncan JL, Roorda A. Relationship between foveal cone structure and clinical measures of visual function in patients with inherited retinal degenerations. *Invest Ophthalmol Vis Sci.* 2013; 54(8):5836–5847. [PubMed: 23908179]
33. Rosenfeld PJ, Durbin MK, Roisman L, et al. ZEISS Angioplex Spectral Domain Optical Coherence Tomography Angiography: Technical Aspects. *Dev Ophthalmol.* 2016; 56:18–29. [PubMed: 27023249]
34. Durbin MK, An L, Shemonski ND, et al. Quantification of retinal Microvascular density in optical coherence tomographic angiography images in diabetic retinopathy. *JAMA Ophthalmol.* 2017; 135(4):370–376. [PubMed: 28301651]
35. Zayit-Soudry S, Duncan JL, Syed R, Menghini M, Roorda AJ. Cone structure imaged with adaptive optics scanning laser ophthalmoscopy in eyes with nonneovascular age-related macular degeneration. *Invest Ophthalmol Vis Sci.* 2013; 54(12):7498–7509. [PubMed: 24135755]
36. Duncan JL, Zhang Y, Gandhi J, et al. High-resolution imaging with adaptive optics in patients with inherited retinal degeneration. *Invest Ophthalmol Vis Sci.* 2007; 48(7):3283–3291. [PubMed: 17591900]
37. Talcott KE, Ratnam K, Sundquist SM, et al. Longitudinal study of cone photoreceptors during retinal degeneration and in response to ciliary neurotrophic factor treatment. *Invest Ophthalmol Vis Sci.* 2011; 52(5):2219–2226. [PubMed: 21087953]
38. Consugar MB, Navarro-Gomez D, Place EM, et al. Panel-based genetic diagnostic testing for inherited eye diseases is highly accurate and reproducible, and more sensitive for variant detection, than exome sequencing. *Genet Med.* 2015; 17(4):253–261. [PubMed: 25412400]
39. Adackapara CA, Sunness JS, Dibbernardo CW, Melia BM, Dagnelie G. Prevalence of cystoid macular edema and stability in oct retinal thickness in eyes with retinitis pigmentosa during a 48-week lutein trial. *Retina.* 2008; 28(1):103–110. [PubMed: 18185146]
40. Hajali M, Fishman GA, Anderson RJ. The prevalence of cystoid macular oedema in retinitis pigmentosa patients determined by optical coherence tomography. *Br J Ophthalmol.* 2008; 92(8): 1065–1068. [PubMed: 18653601]

41. Huckfeldt RM, Comander J. Management of cystoid macular edema in retinitis pigmentosa. *Semin Ophthalmol.* 2017; 32(1):43–51. [PubMed: 27748628]
42. Grunwald JE, Maguire AM, Dupont J. Retinal hemodynamics in retinitis pigmentosa. *Am J Ophthalmol.* 1996; 122(4):502–508. [PubMed: 8862046]
43. Li G, De La Garza B, Shih YY, Muir ER, Duong TQ. Layer-specific blood-flow MRI of retinitis pigmentosa in RCS rats. *Exp Eye Res.* 2012; 101:90–96. [PubMed: 22721720]
44. Zhang Y, Harrison JM, Nateras OS, Chalfin S, Duong TQ. Decreased retinal-choroidal blood flow in retinitis pigmentosa as measured by MRI. *Doc Ophthalmol.* 2013; 126(3):187–197. [PubMed: 23408312]
45. Schmidt KG, Pillunat LE, Kohler K, Flammer J. Ocular pulse amplitude is reduced in patients with advanced retinitis pigmentosa. *Br J Ophthalmol.* 2001; 85(6):678–682. [PubMed: 11371487]
46. Turksever C, Valmaggia C, Orgul S, Schorderet DF, Flammer J, Todorova MG. Retinal vessel oxygen saturation and its correlation with structural changes in retinitis pigmentosa. *Acta Ophthalmol.* 2014; 92(5):454–460. [PubMed: 24767408]
47. Zong Y, Lin L, Yi C, et al. Retinal vessel oxygen saturation and vessel diameter in retinitis pigmentosa at various ages. *Graefes Arch Clin Exp Ophthalmol.* 2016; 254(2):243–252. [PubMed: 25952041]
48. Eysteinson T, Hardarson SH, Bragason D, Stefansson E. Retinal vessel oxygen saturation and vessel diameter in retinitis pigmentosa. *Acta Ophthalmol.* 2014; 92(5):449–453. [PubMed: 24767302]
49. Spaide RF, Fujimoto JG, Waheed NK. Image artifacts in optical coherence tomography angiography. *Retina.* 2015; 35(11):2163–2180. [PubMed: 26428607]
50. Menghini M, Lujan BJ, Zayit-Soudry S, et al. Correlation of outer nuclear layer thickness with cone density values in patients with retinitis pigmentosa and healthy subjects. *Invest Ophthalmol Vis Sci.* 2014; 56(1):372–381. [PubMed: 25515570]
51. Choi SS, Doble N, Hardy JL, et al. In vivo imaging of the photoreceptor mosaic in retinal dystrophies and correlations with visual function. *Invest Ophthalmol Vis Sci.* 2006; 47(5):2080–2092. [PubMed: 16639019]
52. Duncan JL, Biswas P, Kozak I, et al. Ocular phenotype of a family with *FAM161A*-associated retinal degeneration. *Ophthalmic Genet.* 2016; 37(1):44–52. [PubMed: 25007332]
53. Duncan JL, Roorda A, Navani M, et al. Identification of a novel mutation in the *CDHR1* gene in a family with recessive retinal degeneration. *Arch Ophthalmol.* 2012; 130(10):1301–1308. [PubMed: 23044944]
54. Genead MA, Fishman GA, Rha J, et al. Photoreceptor structure and function in patients with congenital achromatopsia. *Invest Ophthalmol Vis Sci.* 2011; 52(10):7298–7308. [PubMed: 21778272]
55. Michaelides M, Rha J, Dees EW, et al. Integrity of the cone photoreceptor mosaic in oligocone trichromacy. *Invest Ophthalmol Vis Sci.* 2011; 52(7):4757–4764. [PubMed: 21436275]
56. Morgan JI, Han G, Klinman E, et al. High-resolution adaptive optics retinal imaging of cellular structure in choroideremia. *Invest Ophthalmol Vis Sci.* 2014; 55(10):6381–6397. [PubMed: 25190651]
57. Sun LW, Johnson RD, Langlo CS, et al. Assessing photoreceptor structure in retinitis pigmentosa and Usher syndrome. *Invest Ophthalmol Vis Sci.* 2016; 57(6):2428–2442. [PubMed: 27145477]
58. Wolfing JI, Chung M, Carroll J, Roorda A, Williams DR. High-resolution retinal imaging of conerod dystrophy. *Ophthalmology.* 2006; 113(6):1014–1019.

## Biography

Young Ju Lew, MD, graduated from the Hanyang University College of Medicine, Seoul, Korea in 2001. In 2006, she completed her ophthalmology residency. After a fellowship at the Kim's Eye Hospital, she has been a retinal specialist at the same hospital since 2007. From 2016 to 2017, she completed her research fellowship at the Department of

Ophthalmology, University of California, San Francisco. Her primary areas of interest are inherited retinal degenerations and retinal imaging.

Author Manuscript

Author Manuscript

Author Manuscript

Author Manuscript

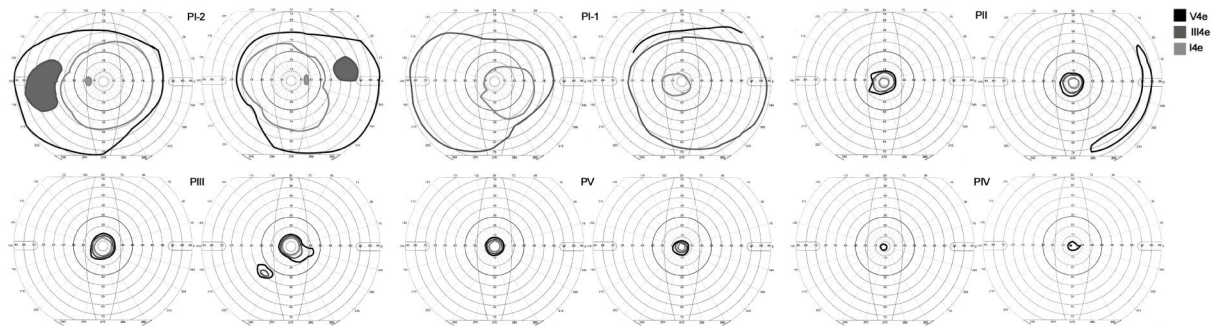


**Figure 1.**

Goldmann visual fields for patients listed in Table 1. RE, right eye; LE, left eye; light gray area: I4e isopter; medium gray area, III4e isopter, dark gray area, V4e isopter. Fields are displayed in order of increasing disease severity from least severe (P I-2, 40126) at the upper left to most severe (P IV, 40123) at the lower right. Shaded areas represent scotomas. The V4e isopter was not tested completely in P I-1 (40116) to avoid patient fatigue as the III4e isopter was full in each eye.

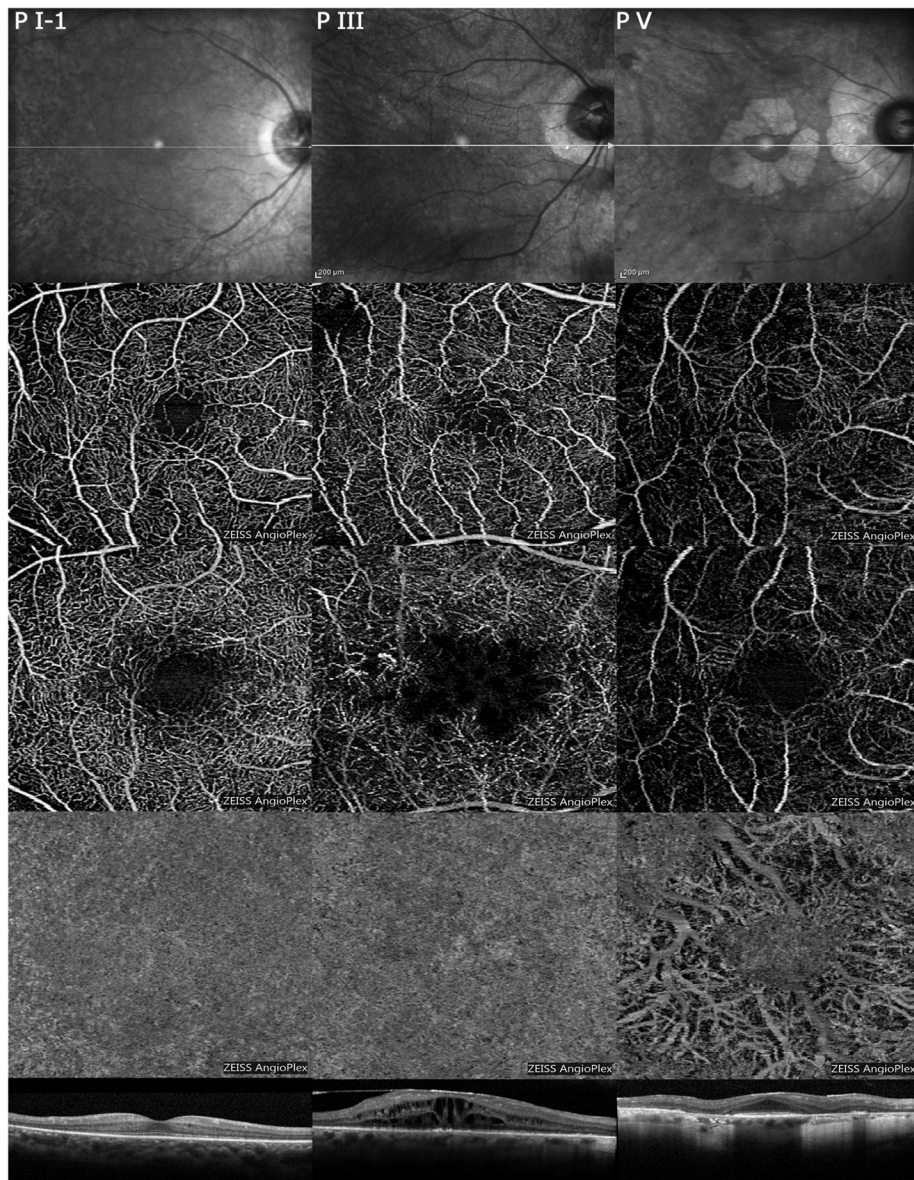


**Figure 2.** Optical coherence tomography angiography (OCTA) and spectral domain optical coherence tomography (SDOCT) images of P I-1 (40116) (left column), P III (middle column) and P V (right column). (Top): infrared fundus images; (Second row): OCTA images from the superficial capillary plexus, deep capillary plexus (Third row) and choriocapillaris (Fourth row) layers; (Bottom): SDOCT B-scan horizontal images corresponding to white lines shown in (Top).

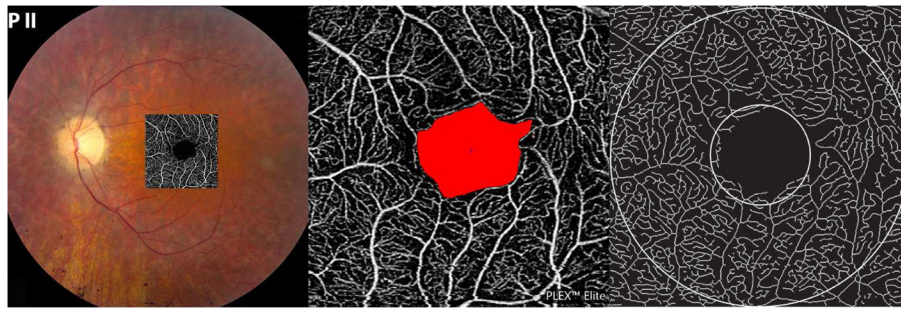


**Figure 3.**

Optical coherence tomography angiography (OCTA) images from P II (40063), left eye. (Left) A  $3 \times 3$  mm superficial capillary plexus (SCP) image is superimposed on color fundus photograph using vascular landmarks to precisely align the images. (Middle) Manual outlining of borders of the foveal avascular zone (FAZ) and identification of FAZ area (shaded red). (Right) Skeletonized images for vessel density of SCP. Vessel density was obtained at foveal and parafoveal area with a diameter 1mm and 3 mm, respectively. Inner circle and outer circle represent 1mm and 3mm in diameter, respectively.



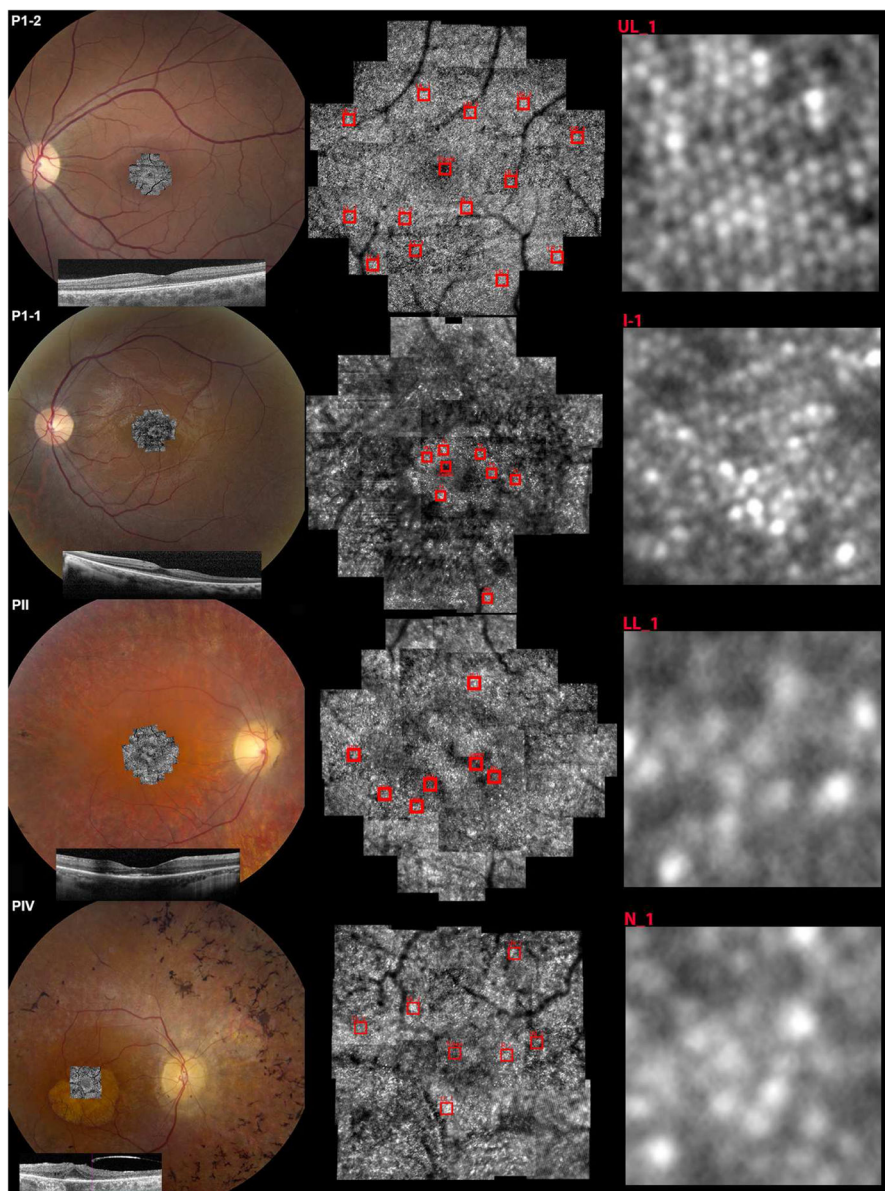


**Figure 4.** AOSLO images from P I-2 (40126) (Top), P I-1 (40116) (Second row), P II (40063) (Third row) and P IV (40123) (Bottom). Left column: AOSLO images are superimposed on color fundus photographs using retinal vascular landmarks to precisely align the images. Cross sectional swept source OCT horizontal B-scans through the fovea are shown at the bottom. Middle column: AOSLO montages with rectangular boxes showing regions of interest for measuring cone spacing. Right column: magnified insets of regions of interest indicated with red boxes in the middle column showing cone photoreceptors as white spots in regular mosaics (top right and second right), and a less regular mosaic with increased cone spacing (third right and bottom right). Patients are arranged in order of increasing disease severity from top to bottom.

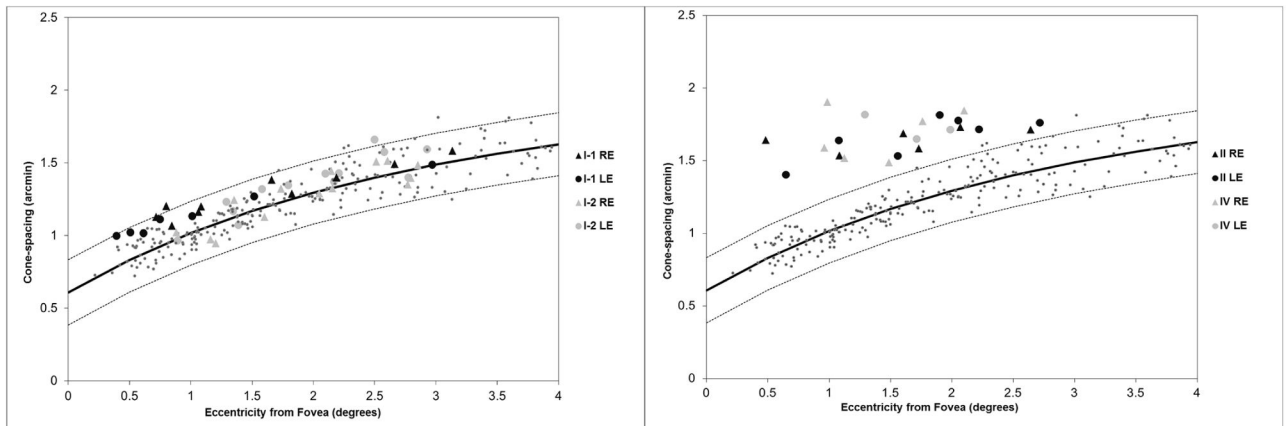


**Figure 5.**

AOSLO cone spacing measures in P I-1 (40116) and P I-2 (40116) are shown in the left panel, while P II (40063) and P IV (40123) are shown in the right panel. Cone photoreceptor spacing was within the 95% confidence limits (dashed lines) of the normal mean (solid lines) at almost all locations in P I-I (40116) and P I-2 (40126) with early disease, and increased above the upper 95% confidence limits at all locations in P II (40063) and P IV (40123) with advanced disease.

Table 1

## Clinical characteristics

ID/Age at exam, years/Sex AOSLO ID	Eye	Visual acuity	Refractive error	Lens status	Ophthalmologic findings	ERG amplitude		MAK Genetic test results
						scotopic	photopic	
P I-1/25/M 40116	RE	20/20 <sup>-1</sup>	-1.50+0.50×110	Clear	Supernasal bone spicules C/D=0.2 (BE)	Not measurable	Reduced by 20–30% with delayed timing	Homozygous c.485C>T, p.Thr162Ile
	LE	20/20 <sup>-1</sup>	-1.75+0.25×082	Clear				
P I-2/31/F 40126	RE	20/13 <sup>-1</sup>	-0.50+0.25×155	Clear	Supernasal bone spicules C/D=0.2 (BE)	Mixed scotopic a- and b-wave reduced by 25–30% with delayed timing	Reduced by 20–30% with delayed timing	Homozygous c.485C>T, p.Thr162Ile
	LE	20/16 <sup>-2</sup>	-0.75+0.25×040	Clear				
P II/46/F 40063	RE	20/32 <sup>-2</sup>	-1.75+1.00×155	I + PSC	Preserved central fovea; bone spicules and cobblestone atrophy anterior to the arcades C/D=0.3 (BE)	Not measurable	Reduced by 95%	Homozygous c.1297_1298insAlu p.Lys433 insAlu
	LE	20/32	-1.75+0.75×015	Trace PSC				
P III/56/M N/A	RE	20/60 <sup>-1</sup>	plano	Pseudophakia	Severe CME, ERM at fovea; peripheral scattered bone spicules and cobblestone RPE atrophy C/D=0.4 (BE)	Not measurable	Not measurable	Homozygous p.Lys429 insAlu_353bp
	LE	20/70 <sup>-1</sup>	plano	Pseudophakia				
P IV/71/F 40123	RE	20/25 <sup>-2</sup>	plano	Pseudophakia	Preserved central foveal island with surrounding RPE atrophy; peripheral scattered bone spicules and cobblestone RPE atrophy C/D=0.5 (BE)	Not measurable	Not measurable	Homozygous p.Lys429 insAlu_353bp
	LE	20/40 <sup>-2</sup>	-1.00+1.25×085	Pseudophakia				
P V/81/M N/A	RE	20/30 <sup>-1</sup>	-1.50+1.00×165	Pseudophakia, capsular opacity and phimosis	Preserved central foveal island with surrounding RPE atrophy; peripheral scattered bone spicules and cobblestone RPE atrophy C/D=0.5 (BE)	Not measurable	Not measurable	Homozygous p.Lys429 insAlu_353bp
	LE	20/25 <sup>-1</sup>	-1.00+0.25×172	Pseudophakia, capsular opacity and phimosis				

ERG, electroretinogram; M, male; F, female; RE, right eye; LE, left eye; BE, both eyes; C/D, cup to disc ratio; PSC, posterior subcapsular cataract, CME, cystoid macular edema; ERM, epiretinal membrane; RPE, retinal pigment epithelium. AOSLO ID numbers are provided for the 4 patients who underwent AOSLO imaging; N/A, not applicable, as the patient was not imaged using AOSLO.

**Table 2**

Quantitative analysis of the vascular density and the FAZ between MAK patients and normal subjects. Significant values are shown in red text. Parafoveal vessel density and perfusion densities of both the superficial and deep capillary plexuses were more reduced in MAK patients, while FAZ area, superficial capillary and deep capillary vessel densities and perfusion densities within 1.0 degrees of the fovea were similar to normal subjects.

	MAK Patients	Normal Subjects	<i>P</i> value
Superficial Capillary Plexus Vessel Density, length/unit area (mm <sup>-1</sup> )			
Center -1.0mm	13.8±5.1	15.2±2.1	0.53
1.0 mm–3.0 mm	17.4±3.0	21.7±0.7	0.012
Deep Capillary Plexus Vessel Density, length/unit area (mm <sup>-1</sup> )			
Center - 1.0 mm	2.9±1.8	2.9±1.6	0.98
1.0 mm–3.0 mm	11.7±4.1	17.9±2.1	0.014
Superficial Capillary Plexus Perfusion Density, perfused area/unit area			
Center -1.0mm	0.29±0.12	0.31±0.04	0.77
1.0 mm–3.0 mm	0.37±0.046	0.43±0.006	0.015
Deep Capillary Plexus Perfusion Density, perfused area/unit area			
Center - 1.0 mm	0.063±0.046	0.035±0.02	0.24
1.0 mm–3.0 mm	0.24±0.073	0.35±0.04	0.013
Foveal Avascular Zone Area, mm <sup>2</sup>			
Superficial Capillary Plexus	0.31±0.18	0.23±0.04	0.80
Deep Capillary Plexus	0.70±0.43	0.48±0.1	